Temperature-Dependent Heterogeneous Efflorescence of Mixed Ammonium Sulfate/Calcium Carbonate Particles

Timothy B. Onasch, Robert McGraw, and Dan Imre*

Atmospheric Sciences Division, Environmental Sciences Department, Brookhaven National Laboratory, Upton, New York 11973

Received: July 5, 2000; In Final Form: September 14, 2000

In this paper, we report observations on single internally mixed ammonium sulfate/calcium carbonate microparticles. Deliquescence and efflorescence relative humidities for this mixed system are reported. The slightly soluble $CaCO_3$ has a negligible effect on the deliquescence relative humidity and the concentration-dependent water activities. Mixed particles at 298 K were observed to exist in two metastable liquid states: (a) supersaturated with respect to both ammonium sulfate and calcium carbonate and (b) supersaturated with respect to ammonium sulfate and saturated with respect to a solid calcium carbonate inclusion. The efflorescence relative humidities differed greatly between the two cases. Solution droplets supersaturated with respect to both salts (no solid inclusion present) effloresced at the homogeneous efflorescence point of pure ammonium sulfate. In contrast, the presence of the calcium carbonate as a ∼500 nm solid inclusion within the 15 μm solution droplets served as a catalyst for heterogeneous nucleation and the particle crystallized at ∼50% relative humidity (RH), a full 13% RH higher than homogeneous efflorescence. A smaller calcium carbonate seed induced efflorescence at an intermediate 47% RH, indicating that the heterogeneous efflorescence rate is a function of the size of the inclusion. The data are analyzed using classical nucleation theory to derive the free-energy barrier to nucleation, the size of the critical nucleus, and the contact parameter between ammonium sulfate and calcium carbonate. The results are compared with available literature. The heterogeneous efflorescence was also investigated as a function of temperature (210−298 K) and found to have only a slight temperature dependence, similar to previous homogeneous efflorescence observations.

1. Introduction

A significant fraction of atmospheric aerosols are observed to be composed of internal mixtures of soluble and insoluble components. Although thermodynamic models are currently successful at predicting the compositions and activities of mixed soluble inorganic salt droplets to high concentrations,[1−3] processes controlling the kinetically hindered phase transitions (e.g., salt efflorescence and ice nucleation) are not well understood. Such liquid−solid phase transitions dramatically change a particle's water content, size, and hence light scattering properties, as well as the chemical reactivity of the surface of the particle. These phase transitions impact the radiative properties[4] and chemistry[5,6] of the atmosphere and may play a determining role in cirrus cloud formation in the upper troposphere.[7,8]

Because of the presence of a solid inclusion, internally mixed particles composed of a soluble salt component and an insoluble or slightly soluble component may exhibit different efflorescence kinetics than externally mixed particles. These solid inclusions may act as heterogeneous sites, catalyzing the crystallization of metastable solutions at lower supersaturations with respect to the solid phase than the supersaturation limit imposed by homogeneous nucleation.[9] As discussed by Han and Martin,[10] field studies indicate that the large supersaturations obtained in laboratory studies of pure aqueous electrolyte droplets such as ammonium nitrate[11−13] are not readily observed in ambient aerosol particles.[14] These results may be evidence of the catalytic effect of internally mixed heterogeneous nuclei. Heterogeneous crystallization represents an alternative mechanism for phase transitions in particles and thus may be an important process that significantly changes the physical properties of atmospheric aerosols. Therefore, to model atmospheric chemistry and climate change, it is essential to understand the kinetics of phase transitions in internally mixed soluble and insoluble salt particles over the full temperature and humidity ranges relevant to the atmosphere.

Probable insoluble components in mixed atmospheric aerosol are soil minerals. Wind-blown dust from deserts and semiarid landscapes can be a significant component of atmospheric aerosols.[4,15] A recent study suggests that the global emission rate of dust particles has dramatically increased due to anthropogenic activities.[16] Particles derived from crustal material usually contain alkaline metals such as K, Ca, and Mg. These crustal species tend to be found in the form of insoluble carbonates.[17,18] Although most mechanically produced particles are coarse and thus have short residence times, a striking example of a smaller, persistent mode is evident in satellite optical depth profiles of Saharan dust clouds in the Caribbean Sea.[19] Recent measurements in the upper troposphere over the continental United States revealed relatively high concentrations of Ca^{2+} in aerosol particles, indicating that crustal material can also be readily transported to high altitudes. Once aloft, particles may become internally mixed through heteromolecular condensation of semivolatile gases, cloud processing, and coagulation. Evidence for such processes can be found in the sea-salt-coated mineral particles observed off the coasts of China.[20,21]

* Corresponding author. E-mail: imre@bnl.gov. Phone: 631-344-4493. Fax: 631-344-2887.

10.1021/jp0024064 CCC: $19.00
Published on Web 10/19/2000

Heterogeneous nucleation has also been implicated in cirrus cloud formation mechanisms. Cirrus clouds are abundant throughout the global troposphere and through their radiative properties have a considerable impact on the climate. Their radiative properties are determined by the number and size distributions of the cloud particles as well as their spatial and temporal coverage. In turn, these microphysical properties may be determined by the freezing mechanisms of the background aerosol. In particular, the initial phase of background particles and the presence of internally mixed solid phases may influence the formation mechanisms of cirrus clouds.[7,8] To date, several groups have carried out studies on the heterogeneous nucleation of aqueous electrolyte droplets as a result of solid inclusions of metal oxides,[10] $CaCO_3$ and $BaSO_4$,[22] and less soluble inorganic salts.[23,24] These previous studies have all been carried out at constant temperature (~298 K).

We have investigated the thermodynamics and kinetics of mixed ammonium sulfate/calcium carbonate particles. Past studies on solution droplet crystallization have shown that single-particle electrodynamic traps can represent a clean and well-characterized environment with which to investigate nucleation. In this paper, we report the deliquescence, water activities, and efflorescence results for mixed ammonium sulfate/calcium carbonate particles as a function of temperature.

2. Experimental Section

2.1. Electrodynamic Trap. The temperature-controlled electrodynamic trap used for this study has been described in detail elsewhere.[25] Briefly, the electrodynamic trap consists of three copper electrodes with hyperboloidal surfaces separated by sapphire spacers. The top and bottom cap electrodes are charged with a dc voltage, and the middle ring electrode is charged with an ac voltage of 50−170 V at 300 Hz. The top electrode has a center plug that can be removed to allow for the introduction of a particle from above and replaced to form an almost seamless inner surface. The ring electrode has four holes of 0.125 in. diameter drilled along the *x* and *y* axes in the horizontal plane. A HeNe laser beam passes along the *x* axis through the trap and illuminates the levitated particle in the center of the trap. The light scattered by the particle is observed with a charge-coupled device (CCD) camera and a photomultiplier tube (PMT) along the *y* axis, 90° from the beam path. The image of the particle observed by the camera is used to adjust the vertical position of the particle within the cell and thus determine the relative composition of the particle. Light scattered by growing or evaporating spherical liquid droplets and collected by the PMT is fitted using Mie theory to determine the size of the droplets and to indicate the presence or absence of a solid inclusion within the droplets. We will subsequently refer to the scattered light intensity as a function of particle size as a Mie spectrum. The electrodynamic trap is set within a high-vacuum chamber. The chamber is enclosed by an insulating vacuum jacket and has a base pressure of 10^{-6} Torr. The temperature of the trap is controlled through contact with a liquid-nitrogen reservoir and resistive heating. The temperature of the trap is measured by silicon diodes (Lake Shore) above and below the particle with an accuracy of ±0.2 K. The two measured temperatures agreed to within 0.4 K for all of the isothermal experiments and the ice line experiments. A slight temperature gradient (≤0.4 K) at low temperatures is due to the low (water) pressure in the chamber and slow thermal conduction through the cell.

2.2. Particle Production. Mixed ammonium sulfate/calcium carbonate salt solutions were prepared by dissolving ammonium sulfate (Puritronic) in deionized water (Millipore) saturated with calcium carbonate (rhombohedric calcite, Kodak). Solutions containing 4% by mass ammonium sulfate were used to generate crystalline particles within the electrodynamic trap with diameters ranging from 4 to 8 μm. The particles were produced using a simple electrospray apparatus. A glass tube, 21 in. long and 0.25 in. in diameter, was pulled to a point and sanded until a small hole was formed at the bottom. This particle gun was then filled with a filtered (20 nm pore size) solution and inserted into the chamber through the opening in the top electrode, with the tip approximately at the same level as the surface of the top electrode. The chamber was back-filled with a positive pressure of filtered (Balston) dry nitrogen during particle production to minimize contamination from room air. The solution was charged at 1500 V dc, and a supermicron (~40 μm) dilute solution droplet was produced by tapping the top of the gun. The generated solution droplets rapidly evaporated in the dry nitrogen environment and immediately crystallized into much smaller solid particles. Typically, one or two particles were trapped. The gun was extracted; the formfitting plug was inserted into the top electrode, and the vacuum chamber was closed. The ac voltage on the center ring electrode was then varied (down and up) to eject all but one particle. This particle was centered within the trap by dropping the ac voltage to <50 V and adjusting the dc voltage until the particle remained within the horizontal plane at low ac voltages.

The amount of calcium carbonate in a particle is determined from the solubility of calcium carbonate in the mixed salt solution and the volume of the trapped particle. The mixed salt solutions used for this study were prepared with two different relative calcium carbonate compositions. The temperature-dependent study was done on particles with a mole ratio of calcium carbonate to ammonium sulfate of $\sim 3.8 \times 10^{-4}$. Particles with relative compositions of $\sim 1.9 \times 10^{-4}$ mol of calcium carbonate to moles ammonium sulfate were also generated for the room-temperature efflorescence study.

2.3. Experimental Procedures. Two types of experiments were performed during this study. The first is a relative humidity (RH) scan at a constant temperature. For this experiment, the temperature of the chamber was set using a programmable temperature controller (Lake Shore), and sufficient time was allowed for the chamber to become equilibrated in temperature. Temperature equilibrium was defined by $\Delta T \leq 0.4$ K as measured by the silicon diodes located above and below the particle on the end cap electrodes. A leak valve (Varian) was then used to introduce water vapor into the chamber from a previously degassed water bulb. Capacitance manometers (Baratron 100 Torr and 1 Torr heads, ±0.08% error of reading) were used to directly measure the total pressure and thus water pressure within the chamber. A data collection system, consisting of a custom LabView (National Instruments) program running on a PC computer, a IEEE-488 interface board, and a multimeter (Keithley 2001), was used to collect and store the temperature, water vapor pressure, volts dc, and scattered light data. The relative humidity was then directly calculated from the temperature and water vapor pressure, with a combined percent error for the relative humidity measurement of 1.0% at 298 K increasing to 2.0% at 210 K. For these experiments, the relative humidity was increased until the ammonium sulfate in the particles had deliquesced at 80% RH. This deliquescence relative humidity is in agreement with literature data for pure ammonium sulfate particles at 298 K.[22,25,26] The calcium carbonate within each particle remained as a solid inclusion at these relative humidities, as the deliquescence relative humidity

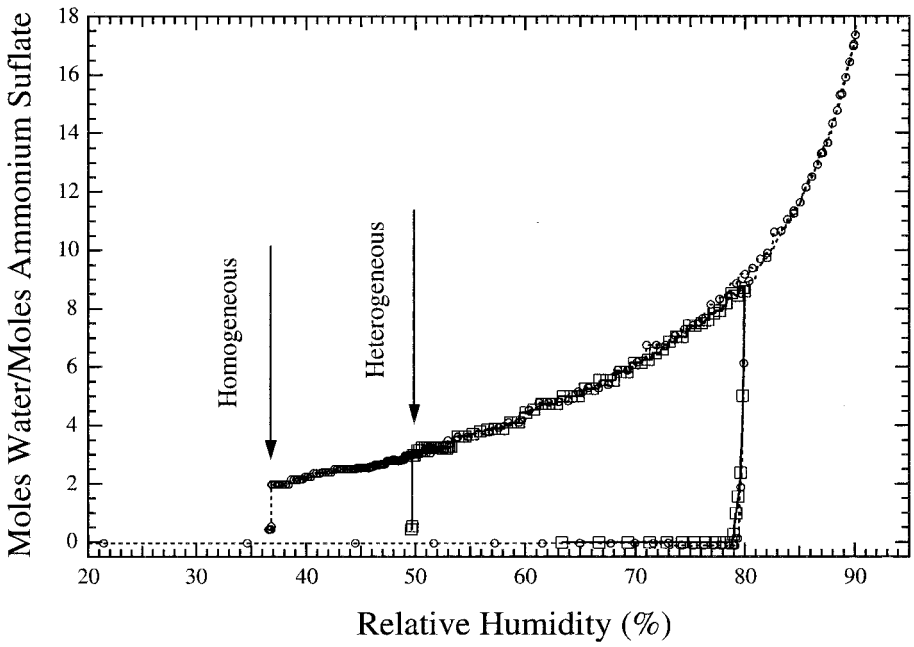

Figure 1. Relative humidity cycles for a single mixed ammonium sulfate/calcium carbonate particle at 298 K. The circles represent a humidity cycle of the particle exposed to a maximum relative humidity of 90%, denoted case 1. Upon a decrease of the relative humidity, the particle effloresced at 37.0% RH, the homogeneous efflorescence point of ammonium sulfate solution droplets. A second humidity cycle, case 2, was carried out on the same mixed salt particle (squares), exposing the solution droplet to a maximum of 80% RH. The observed heterogeneous efflorescence transition for case 2 was 49.7% RH.

for calcium carbonate is estimated to be ~100% RH because of its low solubility. After the ammonium sulfate had fully deliquesced, the relative humidity was then decreased as a function of time by slowly evacuating the chamber through the leak valve. The time rate of change of the relative humidity ranged from −0.0016 to −0.16% RH per second for all experiments. At a much lower relative humidity than the deliquescence RH, the ammonium sulfate effloresced or crystallized back into a solid crystalline form. By performing this type of experiment at several temperatures, the deliquescence and efflorescence RHs as a function of temperature were mapped out.

The second set of experiments was carried out along the ice−solution equilibrium line. For these experiments, a trapped particle was deliquesced at 263 K and hydrated via water condensation. As more water was added, the surfaces of the chamber were eventually coated with ice. Under these conditions, the composition of the solution droplet was in equilibrium with the vapor pressure of ice. The chamber was then filled with extra nitrogen (~100 Torr) to ensure good thermal contact between the chamber walls and the particle. Then, as the temperature was systematically decreased, the water vapor maintained equilibrium with ice by condensation on the chamber walls. The particle composition equilibrates with the water vapor by losing water along the ice−liquid ammonium sulfate equilibrium line as the temperature decreases.

3. Results and Discussion

3.1. Room-Temperature Results. Two hydration/dehydration scans for one individual mixed ammonium sulfate/calcium carbonate particle at 298 K are shown in Figure 1. These curves are nearly identical, except for a difference in their respective efflorescence relative humidities (ERHs). The circles represent a humidity scan, case 1, during which the particle deliquesced and was subsequently exposed to relative humidities as high as 90.1%. The relative humidity was then decreased and the particle effloresced at 37.0% RH, approximately the homogeneous efflorescence relative humidity reported in the literature.[3,22,25,27−30] The square points represent another humidity scan, case 2, in which the same particle was exposed to relative humidities no higher than the deliquescence relative humidity (DRH). Upon a decrease in RH, the particle was observed to effloresce at 49.7% RH. This efflorescence relative humidity is in excellent agreement with our earlier results[22] for the heterogeneous efflorescence of mixed ammonium sulfate/calcium carbonate particles. This dual behavior, dependent upon the maximum RH achieved during the hydration part of a cycle, has been systematically reproduced. A similar strong dependence of the ERH on the maximum relative humidity experienced by an individual particle has also been observed in mixed ammonium nitrate/succinic acid particles.[12]

Curves a and b in Figure 2 correlate with the dehydration runs of cases 2 and 1, respectively. These Mie spectra indicate the highest relative humidities achieved during the two different cases. The sharp increase in scattered light intensity at low RH marks the efflorescence transitions of the solution droplet. Figure 2c shows the results of a calculated spectrum using the relative-humidity-dependent refractive index and density data of pure ammonium sulfate particles at 298 K from Tang and Munkelwitz.[31] The calculated curve was fit to curve b using the initial particle size as the only adjustable parameter. The two experimental curves exhibit the dominant Mie spectra characteristics of a pure ammonium sulfate droplet as illustrated by the excellent agreement with the calculated spectrum.

Aside from the obvious differences between curves a and b in the RH range covered, a careful comparison between the two reveals a high-frequency component in curve a that is absent in curve b. This is particularly noticeable at lower RH, as illustrated in Figure 3, in which the 50−60% RH region of curves a and b is expanded to full scale. This high-frequency signal is the signature of the solid calcium carbonate inclusion within the solution droplet. The increasing amplitude of this signal with decreasing relative humidity is consistent with an increase in seed size as a result of calcium carbonate precipitation.

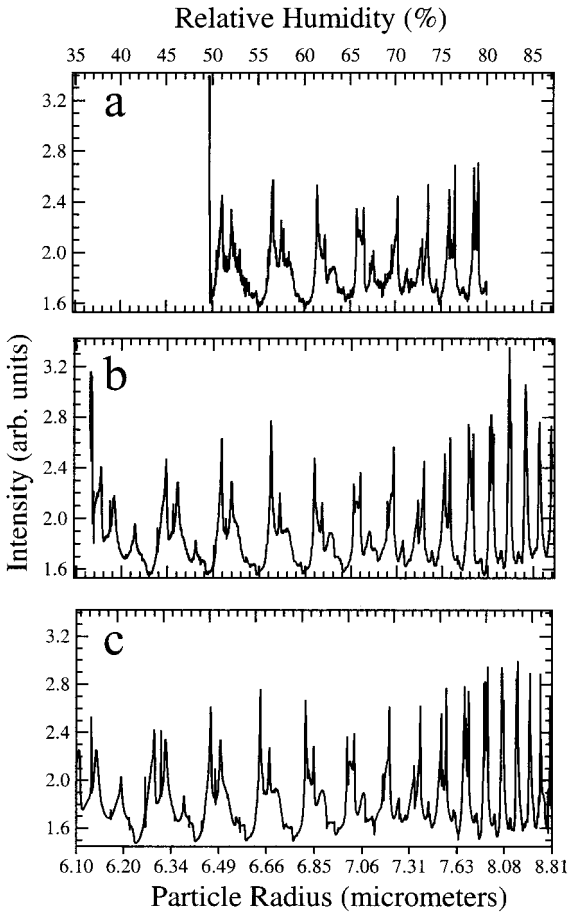

Figure 2. Mie scattering spectra for mixed ammonium sulfate/calcium carbonate solution droplets as a function of decreasing relative humidity: (a) corresponds to case 2, the humidity cycle shown in Figure 1 that reached a maximum relative humidity of 80% RH and effloresced at 49.7% RH; (b) corresponds to case 1, the humidity cycle shown in Figure 1 that reached a maximum relative humidity of 90% RH and effloresced at 37% RH; (c) is a theoretical curve calculated from data given in Tang and Munkelwitz (ref 31).

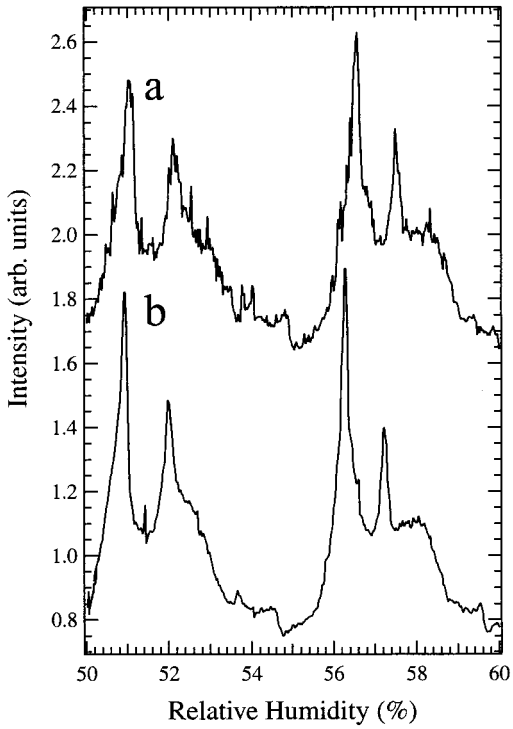

Figure 3. A close-up of the experimental Mie curves shown in Figure 2. The top curve corresponds to (a) in Figure 2 and the bottom curve corresponds to (b). The high-frequency signal due to a solid inclusion is an obvious component of the top curve; however, it is not present in the bottom curve. The curves have been offset along the *y* axis for clarity.

Our interpretation of the observations presented in Figures 1−3 is as follows. During the hydration phase, the calcium carbonate is in equilibrium with the solution and its concentration is determined by its solubility. Thus, more calcium carbonate will be dissolved into solution as the droplet takes up more water at higher relative humidities. For case 1, as the particle is exposed to relative humidities up to 90%, all of the calcium carbonate dissolves as the solution becomes subsaturated with respect to the calcium carbonate precipitate. Upon a decrease in RH, the liquid particle becomes supersaturated with respect to both the ammonium sulfate and the calcium carbonate crystals. Despite the fact that the solution may be more supersaturated with respect to calcium carbonate, the mixed solution droplet is observed to effloresce at the ammonium sulfate homogeneous nucleation relative humidity. Therefore, as observed in case 1, the dissolved calcium carbonate does not affect the kinetics of ammonium sulfate efflorescence. In case 2, in which the maximum relative humidity reached was ∼80%, the solution is saturated with respect to calcium carbonate at all times and a solid inclusion is thus always present. As the relative humidity is decreased, the calcium carbonate precipitates back out of solution onto the existing inclusion. The inclusion then induces heterogeneous efflorescence of ammonium sulfate at 49.7% RH, significantly changing the ammonium sulfate efflorescence kinetics.

To substantiate the above interpretation, it is possible to calculate the RH at which one expects the entire calcium carbonate seed to dissolve. The major uncertainty in this calculation has to do with the phase of calcium carbonate. The thermodynamically stable form of calcium carbonate is calcite; however, calcium carbonate has been observed to exist in five distinct solid phases including a highly soluble amorphous state.[32] Ostwald's rule of stages predicts that the observed crystalline phase precipitated in a solution will be the phase most like the solution, a highly soluble metastable phase.[33] Assuming that our stock solution was saturated with respect to calcite and using literature solubility values for the different phases, the solution droplets at 90% RH are indeed calculated to be subsaturated with respect to the metastable amorphous and the ikaite (hexahydrate) forms, however, not subsaturated with respect to calcite. Therefore, we believe that the calcium carbonate in the mixed solution droplets precipitated out as a metastable phase, either amorphous or ikaite, during crystallization.

Finally, it should be noted that for all runs the observed deliquescence relative humidity at 298 K is 80.0%, in good agreement with literature data for binary ammonium sulfate/water droplets.[3,25] A slight uptake of water prior to deliquescence similar to the uptake noted by Oatis et al.[22] for the mixed ammonium sulfate/calcium carbonate system was also observed. This slight uptake indicates that the calcium carbonate does influence the thermodynamics of the system, similar to the results observed by Tang and Munkelwitz[34] for mixed soluble salt systems; however, the impact is negligible because of the exceedingly small amount of calcium carbonate present in the solution. In addition, the water uptake curves (activity curves) of the mixed ammonium sulfate/calcium carbonate particles agree with the pure ammonium sulfate curves published by Tang

and Munkelwitz[3] and calculated using the mole-fraction-based model of Clegg et al.[1] within experimental errors. The particular uptake curves given in Figure 1 are exceptions. These curves were carried out in a high-ac field to stabilize the particle for optimum Mie scattering data collection. Under high-ac fields, there is a significant force in the vertical direction on the particle such that the derived particle compositions are biased low. However, other experiments carried out for this study under low-ac conditions agree well with previously published data. Therefore, the small amount of calcium carbonate dissolved within the solution, whether saturated or supersaturated, does not appreciably alter the thermodynamics of the solution droplet. This is further supported by the excellent fit of the calculated to the observed Mie scattering spectra shown in Figure 2, where the index of refraction and density used were for pure ammonium sulfate.

3.2. Room-Temperature Analysis. 3.2.1. Homogeneous Nucleation. Following Oatis et al.[22] and Richardson and Snyder,[23] the efflorescence of mixed ammonium sulfate/calcium carbonate particles can be interpreted using classical nucleation theory. We begin by analyzing the homogeneous efflorescence of ammonium sulfate in case 1. The rate of formation of a critical nucleus per unit volume of a droplet can be expressed as

$$J = J_0 \exp(-W^*/kT) \tag{1}$$

where J_0, the kinetic pre-exponential factor, is a measure of the attempt frequency for a molecule in the liquid to become incorporated into the critical nucleus, W^* is the maximum free-energy barrier to transition to the more stable phase, k is the Boltzmann constant, and T is the temperature in K. Classical nucleation theory relates the reduced barrier height to the number of molecules in the critical nucleus, g^*, and the critical supersaturation of the solute, S^*, as follows:

$$\frac{W^*}{kT} = \frac{1}{2} g^* \ln S^* \tag{2}$$

where $S^* = a_{crit}/a_{sat}$ and a_{crit} is the activity of the solute at efflorescence and a_{sat} is the activity of the solute in equilibrium with crystalline ammonium sulfate.[35] Combining these two equations gives

$$J = J_0 \exp\left(-\frac{1}{2} g^* \ln S^*\right) \tag{3}$$

where the nucleation rate, J, and the critical supersaturation, S^*, are determined directly from the experimental data.

Assuming that a single nucleation event occurs in a droplet at efflorescence, the nucleation rate, J, can be determined from the volume of the particle at efflorescence, V_e, and the induction time for the nucleation, t, through the relationship $J = 1/(V_e t)$. The Mie fit shown in Figure 2 gives a very accurate particle size measurement as a function of relative humidity. The induction time, that is, the time spent at constant particle composition prior to nucleation, can be estimated by the time rate of change of the relative humidity (particle composition) during a dehydration run. We estimate an upper limit on the induction time to be ≤ 1 s in all cases observed for this study. The homogeneous nucleation rate for case 1, the supersaturated ammonium sulfate/calcium carbonate solution droplet, is then determined to be 1.0×10^9 cm^{-3} s^{-1}. This represents a lower limit on the homogeneous nucleation rate because of the uncertainty in bounding the induction time. The critical supersaturation at the point of efflorescence is obtained directly from the experimental data using the Gibbs−Duhem relation,

$$\ln S^* = \int_{ERH}^{DRH} x_1/x_2 \, \mathrm{d} \ln \mathrm{RH} \tag{4}$$

where x_1/x_2 is the mole ratio of water to ammonium sulfate in the droplet.[23,22] The critical supersaturations were obtained using the experimentally determined phase transitions and the uptake curve for ammonium sulfate calculated using the thermodynamic model of Clegg et al.[1] For case 1, the critical supersaturation is determined to be 29.9. J_0 is estimated to be 1×10^{32} cm^{-3} s^{-1} from

$$J_0 = n \frac{kT}{h} \exp\left(\frac{-\Delta g}{kT}\right) \tag{5}$$

where n is the molecular concentration in the crystalline ammonium sulfate nucleus (8.1×10^{21} cm^{-3}), h is Planck's constant, kT/h is the jump frequency of molecules from solution to nucleus, and Δg ($\sim 6kT$) is the free-energy barrier to the jump.[23] With these values for a lower limit on the homogeneous nucleation rate, the pre-exponential factor, and the critical supersaturation, we calculate an upper limit on the number of molecules in the critical nucleus to be 31 and an upper limit on the reduced barrier height, W^*/kT, to be 53 for case 1.

The previous analysis does not include any assumptions concerning the shape of the critical nucleus. By assuming a spherical shape for the critical nucleus, the barrier height can be related to the interfacial surface tension between the crystalline ammonium sulfate and the mixed salt solution, σ, as

$$W^* = \frac{16\pi\sigma^3 v^2}{3(kT \ln S^*)^2} \tag{6}$$

where v is the specific volume in the solid.[23] Using this equation, an upper limit on the interfacial surface tension of 55.0 erg/cm^2 is calculated for case 1, homogeneous nucleation.

Several previous studies have published interfacial surface tensions for ammonium sulfate. These studies assumed the shape of the critical nucleus to be either spherical[28] or a solid shape based on the geometry of a unit cell of the ammonium sulfate crystal[36,37] and reported values for σ that range from 33 to 80 erg/cm^2. Although our current value falls into the middle of this range, it is difficult to compare these values because of the different assumptions used in the formulation of the nucleation theory applied by these studies. Therefore, for comparison purposes we have reanalyzed the published data using the above set of equations.

Table 1 is a compiled list of literature reports on the efflorescence of pure ammonium sulfate particles. To compare these results using classical nucleation theory, their homogeneous nucleation rates have to be estimated. The literature data (particle diameter, observation time, and ERH) are used to calculate the volume-dependent nucleation rate, J, observed in each study, and the mole-fraction-based thermodynamic model from Clegg et al.[1] is used to convert the listed ERH values to supersaturations. The errors in the derived supersaturation are relatively minor because of the accurate measurements made for the ERH in all of these cases; however, there are large uncertainties in J because of the inability to accurately estimate the induction times. Therefore, the J values in Table 1 represent lower limits for most of the cases and the following analysis is based on these lower limits.

TABLE 1.

ref	no. of particles	diameter (μm)	observation time (s)	ERH (%)	ln J	ln S^*	g^*	T (K)
37	6	12.0−24.2[a]	1	48	19.6	2.74	51	293
36	2	4	1[c]	36.7[b]	24.1	3.42	26	298
22	N/A	5	60	37	19.4	3.40	27	298
28	4	1	1[c]	34.7	28.3	3.53	24	297
38	1	20−30	1500	48	10.6	2.74	51	297.7
29, 40	size distribn	0.03−0.08	1[d]	38−40	37.3	3.29	29	298
27	size distribn	0.45	30, 1800	33	27.3	3.61	22	298
30	size distribn	0.75	14−133	32	26.5	3.66	21	295
49	3	1	1[c]	32.5[b]	28.3	3.64	22	298
10	size distribn	1	190	35	23.0	3.51	24	298
25	N/A	5	1[c]	37	23.4	3.40	27	298
39	2	30	1200	47.48	11.0	2.77	49	298
3	3	6−8[a]	1[c]	37−40	22.4	3.40	27	298
present data	3	12.3	1[c]	37.0	20.7	3.40	31	298

[a] Dry particle diameters. [b] ERH derived from reported particle composition at the efflorescence point and the thermodynamic model from Clegg et al. (ref 1). [c] Observation times estimated from the reported time rate of change of RH during an experiment. [d] Observation time guessed.

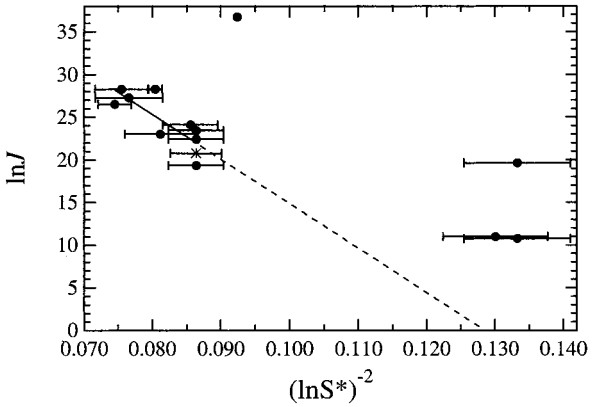

Figure 4. A plot of the supersaturation ((ln S^*)$^{-2}$) versus the estimated nucleation rates (ln J) for the literature data shown in Table 1. The star indicates the value for case 1 from the current study. The solid line is a linear fit to the subset of data that fall below 0.09 on the x axis. The dashed line represents an extrapolation of the linear fit to higher x values. The single data point at (0.092, 36) is from Orr et al. (ref 29) and the three data points near (0.132, 15) are from Cohen et al. (ref 37), Kim et al. (ref 38), and Chan et al. (ref 39).

Combining eq 1 and eq 6, taking the natural logarithm, and rearranging gives

$$\ln J = \ln J_0 - \left[\frac{16\pi\sigma^3 v^2}{3(kT)^3}\right]\frac{1}{(\ln S^*)^2} \qquad (7)$$

which describes the relationship between the nucleation rate and the supersaturation in terms of the surface tension of a spherical nucleus. Figure 4 shows a plot of ln J versus (ln S^*)$^{-2}$ for all of the data listed in Table 1 and the current results for case 1. Although there are large uncertainties in the estimates of the induction time for each experiment, the ERHs and thus the supersaturations are known within a few percent of error. Estimates of the error in supersaturations, taken from either the stated errors in RH measurements in each case or from the statistical spread of the ERH measurements, are given in Figure 4. The results appear to fall into three groups: all of the points below 0.090 on the x axis, the single point at 0.092, and the three points above 0.130. The solid curve in Figure 4 is a best-fit line to the first group of data, with a linear correlation coefficient of −0.8. The ln J_0 derived from the y-intercept of this line is 66.5, in reasonable agreement with the value of ln $J_0 = 71.4$ calculated using eq 5. The surface tension, σ, derived from the slope of this line is 52 erg/cm^2, in excellent agreement with the value obtained from the current data. This fit suggests that all of the data in the first subset are in reasonable agreement with each other and with the results from this study.

The two sets of data that are not well described by this fit are the data from Orr et al.[29] and data from Cohen et al.,[37] Kim et al.,[38] and Chan et al.[39] Although Orr et al.[40] did observe a decreasing ERH with decreasing particle size, the ERHs observed by these authors for very small particles (0.03−0.08 μm in diameter) appear to be too high. For these results to be in reasonable agreement with the first group of data, the induction time must have been extremely long, something not easily accessible in a flowing system. Furthermore, the deliquescence relative humidities reported by these authors are low. Taken together, these discrepancies suggest problems associated with their measurements. These authors provide no error estimates for their ERH measurements. The data in the final group appear to have effloresced at higher relative humidities and thus lower supersaturations than suggested by the fit in Figure 4. This discrepancy may simply be a result of the uncertainty in the estimates of the homogeneous nucleation rates for each experiment. On the other hand, the particles used in these three studies were estimated by the authors to be 12−30 μm in diameter, the largest sizes used in these types of studies. In addition, the numbers of different particles used in these three studies were limited to 6, 1, and 2, respectively. Recent work carried out in our laboratory for ammonium sulfate (unpublished work) and ammonium nitrate[12] particles having diameters between 5 and 15 μm underscores the difficulty in obtaining large particles free from heterogeneous contaminants. Therefore, it is also possible that unknown heterogeneous nuclei may have been present in these large particles and may have induced efflorescence at higher RH and thus lower supersaturation.

Our experimental results combined with a reanalysis of the available literature data for the homogeneous efflorescence of ammonium sulfate particles indicate that the dissolved calcium carbonate does not alter the ammonium sulfate efflorescence kinetics. Furthermore, almost all of the homogeneous efflorescence data for ammonium sulfate droplets appear consistent within the framework of classical homogeneous nucleation theory, despite the different experimental techniques and particle sizes used in each study. However, although classical nucleation theory represents a simple model for predicting and describing the kinetics of phase transitions, our results do not validate the basic assumptions of classical nucleation theory or the assumption of a spherical critical nucleus. Moreover, the results indicate that ammonium sulfate efflorescence experiments have been

TABLE 2

case	no. of particles	impurity diameter (nm)	ERH (%)	S^*	nucleation rate	W^*/kT	g^*
1	3	none	37.0 ± 1.4	29.9	1.0×10^9	53	31
2	16	664	49.4 ± 1.2	14.0	7.2×10^7	33	25
3	8	518	46.6 ± 1.4	16.8	1.2×10^8	32	23

carried out over only a small range of supersaturations and nucleation rates, and thus more experiments are needed in order to fully understand the efflorescence kinetics and clearly test classical homogeneous nucleation theory.

3.2.2. Heterogeneous Nucleation. The heterogeneous efflorescence of the mixed ammonium sulfate/calcium carbonate particles can be analyzed in a similar manner. In addition to case 2 discussed above, mixed ammonium sulfate/calcium carbonate particles with half the calcium carbonate mass of that used in case 2 were produced and their efflorescence was studied. We will refer to these experiments as case 3. From eq 3 and Turnbull,[41] the heterogeneous nucleation per unit surface area of the catalytic inclusion, I, is

$$I = I_0 \exp\left(-\frac{1}{2} g^* \ln S^*\right) \tag{8}$$

The critical supersaturations are determined from the experimental data using eq 4. Assuming that a single nucleation event occurs on the seed at efflorescence, that the phase of the calcium carbonate inclusion is ikaite, and that the ikaite impurity is spherical, the heterogeneous nucleation rates ($cm^{-2}\ s^{-1}$) for cases 2 and 3 can be estimated from the surface area of the calcium carbonate inclusion and the induction time. The induction time estimate is an upper limit, and thus all of the subsequently derived parameters represent limits as well. The surface area of the calcium carbonate inclusion is calculated using the droplet volume at deliquescence, the density of a saturated ammonium sulfate solution,[42] and published solubilities and densities of calcite and ikaite.[43,32] I_0 is estimated to be $10^{22}\ cm^{-2}\ s^{-1}$.[44] The derived impurity diameters, critical supersaturations, nucleation rates, reduced barrier heights, and critical nucleus sizes for cases 1−3 are all presented in Table 2. A comparison of these data clearly shows that the heterogeneous nucleation rate has been changed in similar-sized droplets by varying the solid inclusion mass and thus surface area.

For the heterogeneous cases, the barrier height, W^*, in eq 6 is reduced by a factor that takes into account the catalytic surface of the calcium carbonate inclusion. The factor, $f(\theta) = (\cos^3\theta - 3\cos\theta + 2)/4$, was derived for a spherical nucleus sitting on top of the flat catalytic surface, where θ is the contact angle between the nucleus and the catalyst.[23] The contact angle is related to the surface tensions (σ) between the catalytic inclusion (c), the solid ammonium sulfate nucleus (s), and the mixed salt solution (l) by $\cos(\theta) = (\sigma_{cl} - \sigma_{cs})/\sigma_{sl}$. Because the surface tension, σ_{sl}, between the crystalline ammonium sulfate nucleus and the supersaturated solution has been determined from the homogeneous case, eq 6 modified by the $f(\theta)$ factor can be solved for the contact angle. Contact angles of 80 and 84° are derived from the modified eq 6 for cases 2 and 3, respectively. The similarity between these derived contact angles suggests that the shape and the surface tension of the critical nucleus remain fairly constant over a range of supersaturations, as previously concluded from the homogeneous efflorescence analysis.

The measured heterogeneous efflorescence relative humidity for case 2 agrees very well with the heterogeneous ERH reported by Oatis et al.,[22] and the derived contact angles are similar (80 vs 86°, respectively). The improvement in the current study is the addition of a very accurate measurement of the particle size at efflorescence and deliquescence and thus more accurate values for the mass of calcium carbonate within each particle. This addition is important, as our present results indicate that it is necessary to know the surface area of an inclusion in order to compare the catalytic efficiencies of a solid inclusion with another chemically different substrate.

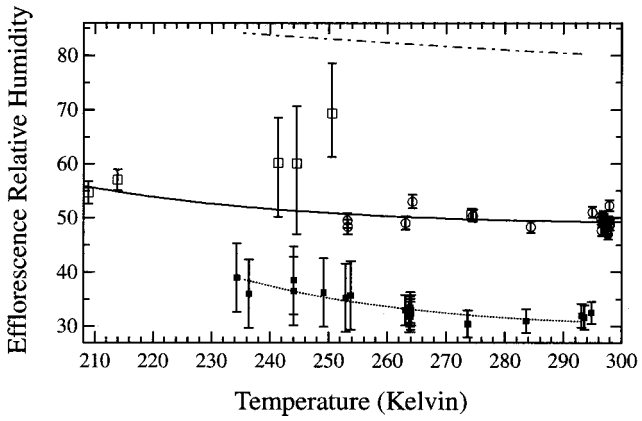

Figure 5. The efflorescence relative humidities for ammonium sulfate particles as a function of temperature. The open symbols are the present study's data for ammonium sulfate particles containing a calcium carbonate inclusion. The solid dots are ammonium sulfate homogeneous efflorescence data from Onasch et al. (ref 30). The top dash−dot line is the deliquescence relative humidity curve determined from Clegg et al. (ref 1).

3.3. Temperature-Dependent Results. Figure 5 shows the observed heterogeneous efflorescence points of mixed ammonium sulfate/calcium carbonate particles as a function of temperature. For comparison, the deliquescence line[1] and the homogeneous efflorescence points[30] have also been included. In all of these experiments, the maximum relative humidity achieved during a hydration cycle was the deliquescence relative humidity at the given temperature. The relative humidities were intentionally kept below 84% so that the calcium carbonate would not fully dissolve, and the observed efflorescence was thus influenced by the presence of a solid calcium carbonate inclusion. The data are divided into three groups based on the experimental procedures used. These groups are discussed separately below. The first category includes all of the experiments above 253 K, the second covers the three points between 240 and 253 K, and the third contains the two data points at ∼210 K.

All of the experiments conducted above 253 K were isothermal experiments in which the relative humidity was decreased until the particles effloresced. The efflorescence product in all cases was the anhydrous ammonium sulfate crystalline phase. The error bars shown in Figure 5 for these experiments are based on the error in relative humidity calculated in section 2.3. In one experiment at 274 K, fragmentation upon efflorescence was observed.

In contrast, during the experiments carried out below 253 K (squares), including all of the data in both the second and third groups, the particles were observed to fragment into several smaller particles at their respective phase transitions. We currently do not have an explanation for this apparent difference in nucleation mechanisms. The daughter particles were determined to be crystalline, as their mass did not change with relative humidity. Note that 253 K is nearly identical to the

observed eutectic point for ammonium sulfate (253.8 K).[25] Below the eutectic point, Xu et al.[25] observed the formation of ammonium tetrahydrate, which was found to have an incongruent melting temperature very near that of the eutectic. To test whether the daughter particles were ammonium sulfate tetrahydrate, they were warmed above the eutectic temperature at low relative humidities, at which a solid-to-solid (tetrahydrate-to-anhydrous) phase transition should occur. However, no evidence of this solid−solid phase transition was found, indicating that the daughter particles had effloresced to the anhydrous crystal.

The second group was obtained by cooling the chamber to temperatures below 253 K. The objective was to reach a target temperature below 253 K and then proceed with an isothermal experimental as described above; however, all of the particles split while cooling. The cooling rate was ~0.5 K/min. During the cooling process, the pressure was simultaneously decreased to keep the relative humidity constant and the water vapor pressure below the frost point of the chamber's walls. Because of the low water pressures (no nitrogen was added for these experiments) and the slow heat conduction, the difference in temperatures above and below the particle reached as high as 4.4 K during cooling. This large temperature gradient is reflected in the large error bars on these data points shown in Figure 5. Although this temperature gradient was not enough to induce ice nucleation at these temperatures, we are not certain of the temperature of the particles when they broke up or whether the splitting occurred at the efflorescence transition. Therefore, these results are omitted from the temperature-dependent analysis.

The two coldest points, composing the third group, were carried out under ice-equilibrium conditions. As described in the Experimental Section, ice was formed on the walls of the chamber and the temperature of the trap was cooled slowly enough to remain in equilibrium with the ice vapor pressure. To ensure good thermal conduction within the trap, approximately 100 Torr of nitrogen was introduced into the cell. Therefore, the efflorescence relative humidities for these particles were determined from the experimentally determined temperature and the ice vapor pressure derived from a thermodynamic model.[1] Although these particles were observed to split, the resulting efflorescence points along the ice−solution equilibrium line are reasonably reproducible. Furthermore, one particle at 274 K also was observed to split into daughter particles at efflorescence, suggesting that although the splitting mechanism may be more prevalent at colder temperatures, it does not exclusively happen below 253 K and it appears to occur at the efflorescence phase transition. Therefore, the ice−solution equilibrium points are included in the following analysis.

3.4. Temperature-Dependent Analysis. The relative humidities for the heterogeneously induced efflorescence of the mixed ammonium sulfate/calcium carbonate particles appear to be almost constant as a function of temperature, rising slightly in RH with decreasing temperature. Figure 5 shows that the homogeneous efflorescence[30] (solid squares) and the current heterogeneous efflorescence (open circles) points track the changes of the deliquescence curve with temperature. This behavior can be explained in terms of the thermodynamics of the system.

Extending the work of Tang and Munkelwitz[26] and Wexler and Seinfeld,[45] Onasch et al.[46] derive the following thermodynamic equation that relates the temperature-dependent water vapor pressure over a salt solution droplet to the enthalpy of vaporization of liquid water, ΔH_v, the enthalpy of solution of the ammonium sulfate salt, ΔH_s, and the total enthalpy of formation of the surface of a critical nucleus, $\Delta H_{surface}$:

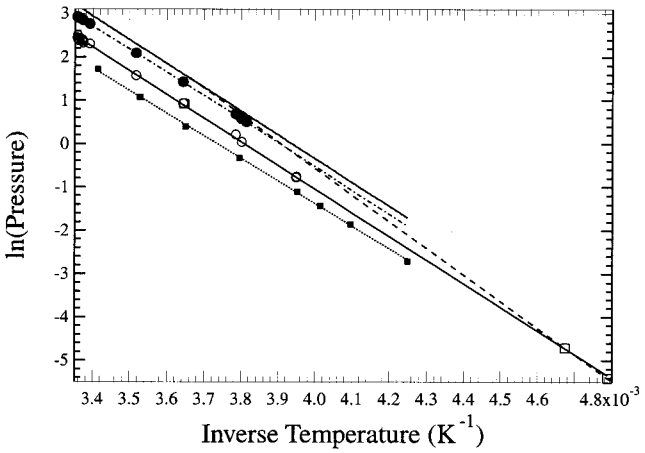

Figure 6. The top solid line is the water saturation vapor pressure and the dashed line is the ice saturation vapor pressure curve, both calculated from Clegg et al. (ref 1). The solid circles are the current deliquescence data with a linear fit, and the open symbols are the current heterogeneous efflorescence data with a linear fit. The solid dots are the homogeneous nucleation data from Onasch et al. (ref 30). Note that all of the lines, except the ice−solution equilibrium line (dashed), are nearly parallel.

$$\frac{\mathrm{d}\ln p_1}{\mathrm{d}T} = \frac{\Delta H_v}{kT^2} - \frac{x_2}{x_1}\frac{\Delta H_s}{kT^2} - \frac{x_2}{x_1}\frac{\Delta H_{surface}}{g^* kT^2} \qquad (9)$$

where g^* is the number of molecules within the critical nucleus, x is a mole fraction, and the subscripts 1 and 2 represent water and ammonium sulfate, respectively. Figure 6 plots the temperature-dependent water saturation,[1] deliquescence,[25] homogeneous efflorescence,[30] and the current heterogeneous efflorescence curves from ammonium sulfate in ln P versus $1/T$ space. The enthalpy of vaporization (~45 kJ/mol) can be determined directly from the slope of the water saturation line (slope = −5470 ± 10). The enthalpy of vaporization term in eq 9 also dominates the temperature-dependent deliquescence curve. Thus, the deliquescence curve[30] (slope = −5400 ± 18) shown in Figure 6 nearly parallels the water saturation curve as a function of temperature, with the difference in slopes being a direct function of the enthalpy of solution of ammonium sulfate (~5.7 kJ/mol) and the mole ratio of ammonium sulfate to water at the deliquescence transition. Equation 9 further indicates that the difference between the slopes of the deliquescence line and the efflorescence curves is a function of the total surface enthalpy per molecule within the critical nucleus[46] for both the homogeneous and heterogeneous cases. Because the efflorescence curves ($\text{slope}_{homogeneous}$ = −5230 ± 31, $\text{slope}_{heterogeneous}$ = −5450 ± 10) parallel the deliquescence curve, the total surface enthalpy per molecule within the critical nucleus must be relatively small.

All of the experiments carried out for this study were done using similar-sized particles (volumes were within a factor of 5) and observation times at a given composition (similar rates of change of RH with time). Therefore, the nucleation rates, and hence the reduced barrier height, W^*/kT, observed for each run were approximately constant. Equation 8 shows that the heterogeneous nucleation rate for efflorescence is a function of the supersaturation of the solution droplet. Using the reduced barrier height and the contact angle calculated for the room-temperature case 2 and eq 6, the surface tension of the

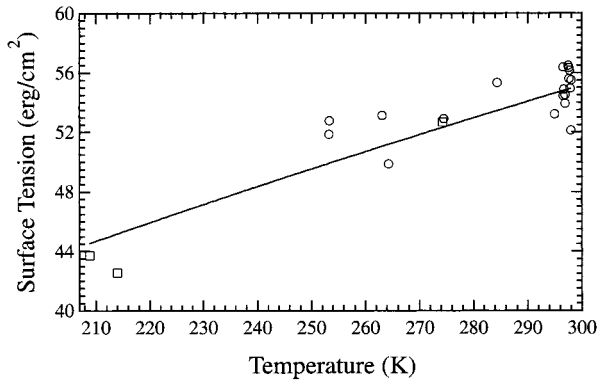

Figure 7. The open symbols represent the temperature-dependent surface tensions of the critical nucleus of crystalline ammonium sulfate as calculated from the heterogeneous efflorescence data. The surface tension increases slightly with increasing temperature. The solid line represents a fit to the data.

ammonium sulfate critical nucleus as a function of temperature is

$$\sigma(T) = \left[\frac{3(kT)^3(\ln S^*)^2}{16\pi v^2 f(\theta)}\left(\frac{W^*}{kT}\right)\right]^{1/3} \quad (10)$$

The supersaturation, S^*, as a function of temperature for the heterogeneous efflorescence data has been determined using experimental efflorescence data and the thermodynamic model developed by Clegg et al.[1] The calculated supersaturation necessary to induce heterogeneous efflorescence increases slightly with decreasing temperature. Figure 7 shows the surface tension as a function of temperature derived by using eq 10 for all of the experimental heterogeneous nucleation points. Classical nucleation theory assumes a temperature- and curvature-independent surface tension; however, the results in Figure 7 indicate that the surface tension for the ammonium sulfate critical nucleus increases slightly with increasing temperature, in qualitative agreement with previous studies on the crystallization of mercury[41] and water.[47] The surface tension is believed to have a weak temperature dependence that is driven by an increasingly negative interfacial entropy with increasing temperature.[47] Huang and Bartell[47] modeled the temperature-dependent surface tension as

$$\sigma = \sigma_0(T/T_0)^n \quad (11)$$

where σ_0 is the surface tension at T_0 (taken to be 55 erg/cm^2 and 298 K, respectively) and n is a fraction <1. Using eq 11 to fit the temperature-dependent data shown in Figure 7 (solid line), we derive a value of $n \approx 0.6$. In comparison, Turnbull[41] and Huang and Bartell[47] found eq 9 to adequately represent data for mercury and water−ice, respectively, with n between 0.3 and 0.4.

The above interpretation of the temperature-dependent data relies on an understanding of the temperature-dependent solubility of the calcium carbonate inclusion. As discussed previously, the phase of the solid calcium carbonate seed in the particles is either an amorphous or hexahydrate crystal. The temperature dependence of the solubility for these two phases differs.[32] The solubility of amorphous calcium carbonate increases by ∼35% over the temperature range from 298 to 250 K and then decreases again to 210 K, whereas the hexahydrate decreases in solubility by ∼94%. However, because the solubilities are so small, the differences in the calculated surface area of the inclusion vary by less than 5% for both phases. Therefore, although we are not certain of the phase of the calcium carbonate, the surface area of the calcium carbonate inclusion (assumed to have the same composition in all cases), and hence the nucleation rate, remains nearly constant over the temperature range investigated in this study.

4. Conclusions

We have investigated the thermodynamics and kinetics of mixed ammonium sulfate/calcium carbonate particles as a function of temperature. The mixed salt droplets were observed to exist in two metastable liquid states supersaturated with respect to at least one crystal: (a) a homogeneous solution droplet that was supersaturated with respect to both crystalline ammonium sulfate and calcium carbonate and (b) a solution droplet with a solid inclusion of calcium carbonate. In state b, the droplet was saturated with respect to calcium carbonate and supersaturated with respect to ammonium sulfate anhydrous crystals.

The slightly soluble calcium carbonate exhibited a negligible impact on the thermodynamics of 15 μm ammonium sulfate droplets from 298 to 263 K. Efflorescence behavior, however, showed a dramatic difference depending upon whether the droplet was initially in state a or state b. In state a, a homogeneous solution droplet, the mixed salt droplet was observed to effloresce at the homogeneous efflorescence relative humidity of pure ammonium sulfate. This result was found to be in good agreement with past experiments, including experiments carried out on a size distribution of small (∼0.5 μm diameter) particles in flow tube experiments. Classical nucleation theory was used to determine limits on the free-energy barrier to efflorescence, the critical nucleus size, and the surface tension of the nucleus for the mixed salt solution droplet in state a. A reanalysis of the available literature data indicates that most of the homogeneous efflorescence results are consistent within the framework of classical nucleation theory.

In contrast, for a droplet in state b, the presence of the calcium carbonate as a solid ∼500 nm inclusion within the 15 μm solution droplet served as a catalyst for heterogeneous nucleation and the particle crystallized at 49.7% RH, approximately 13% higher than the value for homogeneous efflorescence. A smaller calcium carbonate seed (i.e., less surface area) with half the calcium carbonate mass induced nucleation at an intermediate 47% RH. These data were also analyzed using classical nucleation theory to derive limits on the free-energy barrier to nucleation, the size of the critical nucleus, and the contact parameter between ammonium sulfate and calcium carbonate. The heterogeneous data show that the nucleation rate is indeed dependent upon the surface area of the solid inclusion, and thus it is essential to know the surface area of the inclusion in order to determine the efficiency of a solid substrate for inducing heterogeneous crystallization. Furthermore, these experiments show that the heterogeneous nucleation rates can be systematically varied in a single-particle trap system, and thus electrodynamic balances can be used to investigate not only the thermodynamics but also the kinetics of phase transitions over a range of supersaturations.

The observed difference in nucleation mechanisms indicates that the modeling of atmospheric aerosols is further complicated by the presence and amount of insoluble/slightly soluble components. Although small amounts of insoluble/slightly soluble components internally mixed within a soluble salt particle may not significantly influence the thermodynamics of the particle, the addition may have a dramatic effect on the kinetics of crystallization and hence the phase of atmospheric

aerosols. To model the physical properties of soluble salt particles, past research has shown that it is necessary to know the composition and relative humidity histories. Our results indicate that it is further necessary to know the amounts and solubilities of insoluble/slightly soluble components, such as calcium carbonate, to accurately model the phase and thus the size and optical properties of particles that may heterogeneously effloresce.

The heterogeneous efflorescence of mixed ammonium sulfate/calcium carbonate particles was also investigated as a function of temperature (210−298 K). Despite uncertainty in the phase of the calcium carbonate, the calculated surface areas of the solid calcium carbonate inclusions were approximately constant over the temperature range. Therefore, these experiments represent a trajectory of constant nucleation rate as a function of temperature. The heterogeneous efflorescence relative humidity was observed to increase slightly with decreasing temperature down to the ice−solution equilibrium point. This temperature-dependent behavior is very similar to that of ammonium sulfate deliquescence and homogeneous efflorescence. This similarity indicates that the temperature dependence of the heterogeneous efflorescence of mixed ammonium sulfate/calcium carbonate particles is strongly dominated by the enthalpy of solution of the ammonium sulfate salt (and enthalpy of vaporization of water) and that the total surface enthalpy of the critical nucleus is thus a minor component. Classical nucleation theory was used to derive the temperature dependence of the surface tension of the critical nucleus, which exhibited a slight decrease with decreasing temperature. Although this result appears to be consistent with a power law temperature dependence noted by previous authors, the spread in the observed efflorescence data points complicates our ability to uniquely determine the temperature dependence. These data represent our best efforts; however, they are currently not accurate enough to truly test the classical nucleation theories. Further work is necessary to increase experimental accuracy and extend the measurements over wider temperature ranges and supersaturations.

Finally, past research[30,48] shows that the pure ammonium sulfate/water aerosol system has very little temperature dependence of its deliquescence and efflorescence points. We have also observed only a slight temperature dependence in the heterogeneous nucleation of mixed ammonium sulfate/calcium carbonate particles. Our results suggest that the temperature dependence of heterogeneously induced efflorescence depends on the surface area and efficiency of the catalytic substance as well as the temperature dependence of homogeneous nucleation. Therefore, it may be practical to model temperature-dependent heterogeneous efflorescence given room temperature measurements for a given slightly soluble or insoluble component and the knowledge of the temperature dependence of homogeneous efflorescence.

Acknowledgment. This work was supported by the U.S. Department of Energy (Contract DE-AC02-98CH10886). T.B.O. was supported by a Alexander Hollaender Distinguished Postdoctoral Fellowship that is sponsored by the U.S. Department of Energy, Office of Biological and Environmental Research, and administered by the Oak Ridge Institute for Science and Education. T.B.O. thanks Dan Cziczo for reading the manuscript and providing helpful comments.

References and Notes

(1) Clegg, S. L.; Brimblecombe, P.; Wexler, A. S. *J. Phys. Chem.* **1998**, *102A*, 2137.
(2) Zhang, Y.; Seigneur, C.; Seinfeld, J. H.; Jacobson, M.; Clegg, S. L.; Binkowski, F. S. *Atmos. Environ.* **2000**, *34*, 117.
(3) Tang, I. N.; Munkelwitz, H. R. *J. Geophys. Res.* **1994**, *99*, 18801.
(4) Seinfeld, J. H.; Pandis, S. N. *Atmospheric Chemistry and Physics*: *From Air Pollution to Climate Change*; John Wiley & Sons: New York, 1998.
(5) Hu, J. H.; Abbatt, J. P. D. *J. Phys. Chem. A* **1997**, *101*, 871.
(6) Mozurkewich, M.; Calvert, J. G. *J. Geophys. Res.* **1988**, *93*, 15889.
(7) Martin, S. T. *Geophys. Res. Lett.* **1998**, *25*, 1657.
(8) Tabazadeh, A.; Toon, O. B. *Geophys. Res. Lett.* **1998**, *25*, 1379.
(9) Vonnegut, B. *J. Colloid Interface Sci.* **1948**, *3*, 563.
(10) Han, J.-H.; Martin, S. T. *J. Geophys. Res.* **1999**, *104*, 3543.
(11) Richardson, C. B.; Hightower, R. L. *Atmos. Environ.* **1987**, *21*, 971.
(12) Lightstone, J. M.; Onasch, T. B.; Imre, D.; Oatis, S. *J. Phys. Chem.*, in press.
(13) Cziczo, D. J.; Abbatt, J. P. D. *J. Phys. Chem.* **2000**, *104A*, 2038.
(14) Rood, M. J.; Shaw, M. A.; Larson, T. V.; Covert, D. S. *Nature* **1989**, *337*, 537.
(15) Gomes, L.; Gillette, D. A. *Atmos. Environ.* **1993**, *27*, 2539.
(16) Tegen, I.; Lacis, A. A.; Fung, I. *Nature* **1996**, *380*, 419.
(17) Gillette, D. A.; Stensland, G. J.; Williams, A. L.; Barnard, W.; Gatz, D.; Sinclair, P. C.; Johnson, T. C. *Biogeochem. Cycles* **1992**, *6*, 437.
(18) Andronova, A. V.; Gomes, L.; Smirnov, V. V.; Ivanov, A. B.; Shukurova, L. M. *Atmos. Environ.* **1993**, *27A*, 2487.
(19) Li, X.; Maring, H.; Savoie, D.; Voss, K.; Prospero, J. M. *Nature* **1996**, *380*, 416.
(20) Fan, X.-B.; Okada, K.; Niimura, N.; Kai, K.; Arao, K. *Atmos. Environ.* **1996**, *30*, 347.
(21) Zhou, M.; Okada, K.; Qian, F.; Wu, P. M.; Su, L.; Casareto, B. E. *Atmos. Res.* **1996**, *40*, 19.
(22) Oatis, S.; McGraw, R.; Imre, D.; Xu, J. *Geophys. Res. Lett.* **1998**, *25*, 4469.
(23) Richardson, C. B.; Snyder, T. D. *Langmuir* **1994**, *10*, 2462.
(24) Snyder, T. D.; Richardson, C. B. *Langmuir* **1993**, *9*, 347.
(25) Xu, J.; Imre, D.; McGraw, R.; Tang, I. *J. Phys. Chem.* **1998**, *102B*, 7462.
(26) Tang, I. N.; Munkelwitz, H. R. *Atmos. Environ.* **1993**, *27A*, 467.
(27) Cziczo, D. J.; Nowak, J. B.; Hu, J. H.; Abbatt, J. P. D. *J. Geophys. Res.* **1997**, *102*, 18843.
(28) Richardson, C. B.; Spann, J. F. *J. Aerosol Sci.* **1984**, *15*, 563.
(29) Orr, C., Jr.; Hurd, F. K.; Corbett, W. J. *J. Colloid Sci.* **1958**, *13*, 472.
(30) Onasch, T. B.; Siefert, R. L.; Brooks, S. D.; Prenni, A. J.; Murray, B.; Wilson, M. A.; Tolbert, M. A. *J. Geophys. Res.* **1999**, *104*, 21317.
(31) Tang, I. N.; Munkelwitz, H. R. *J. Colloid Interface Sci.* **1991**, *141*, 109.
(32) Gal, J. Y.; Bollinger, J. C.; Tolosa, H.; Gache, N. *Talanta* **1996**, *43*, 1497.
(33) Pokrovsky, O. S. *J. Cryst. Growth* **1998**, *186*, 233.
(34) Tang, I. N.; Munkelwitz, H. R. *J. Appl. Meteorol.* **1994**, *33*, 791.
(35) McGraw, R.; Laaksonen, A. *Phys. Rev. Lett.* **1996**, *76*, 2754.
(36) Tang, I. N.; Munkelwitz, H. R. *J. Colloid Interface Sci.* **1984**, *98*, 430.
(37) Cohen, M. D.; Flagan, R. C.; Seinfeld, J. H. *J. Phys. Chem.* **1987**, *91*, 4583.
(38) Kim, Y. P.; Pun, B. K.-L.; Chan, C. K.; Flagan, R. C.; Seinfeld, J. H. *Aerosol Sci. Technol.* **1994**, *20*, 275.
(39) Chan, C. K.; Flagan, R. C.; Seinfeld, J. H. *Atmos. Environ.* **1992**, *26A*, 1661.
(40) Orr, C.; Hurd, F. K.; Hendrix, W. P.; Junge, C. *J. Meteorol.* **1958**, *15*, 240.
(41) Turnbull, D. J. *J. Chem. Phys.* **1952**, *20*, 411.
(42) Tang, I. N. *J. Geophys. Res.* **1997**, *102*, 1883.
(43) *CRC Handbook of Chemistry and Physics*; Weast, R. C., Ed.; CRC Press Inc.: Boca Raton, FL, 1987.
(44) Newkirk, J. B.; Turnbull, D. *J. Appl. Phys.* **1955**, *26*, 579.
(45) Wexler, A. S.; Seinfeld, J. H. *Atmos. Environ.* **1991**, *25A*, 2731.
(46) Onasch, T. B.; McGraw, R.; Prenni, A. J.; Tolbert, M. A.; Imre, D. 15th International Conference on Nucleation and Atmospheric Aerosols, Rolla, MO, 2000.
(47) Huang, J.; Bartell, L. S. *J. Phys. Chem.* **1995**, *99*, 3924.
(48) Cziczo, D. J.; Abbatt, J. P. D. *J. Geophys. Res.* **1999**, *104*, 13781.
(49) Myerson, A. S.; Izmailov, A. F.; Na, H.-S. *J. Cryst. Growth* **1996**, *166*, 981.